International Journal of
Flow Control

Volume 1 · Number 2 · June 2009

Multi-Science Publishing
ISSN 1756-8250

International Journal of
Flow Control

Volume 1 · Number 2 · June 2009

Effects of Active Control on the Flow Structure in a High Reynolds Number Supersonic Jet

Jin-Hwa Kim and Mo Samimy[1]
Gas Dynamics and Turbulence Laboratory, Department of Mechanical Engineering,
The Ohio State University, GDTL/AARL, 2300 West Case Road,
Columbus, Ohio 43235-7531USA

Abstract

A supersonic axisymmetric jet of design Mach number 1.3 operated in perfectly- and imperfectly-expanded flow regimes is excited by using localized arc filament plasma actuators (LAFPAs). The jet is operated at three fully-expanded jet Mach numbers (M_J) of 1.2 (over-expanded), 1.3 (perfectly-expanded), and 1.4 (under-expanded). The Reynolds number based on the jet diameter and jet exit velocity ranges from $1.1x10^6$ to $1.4x10^6$. Eight equally-spaced LAFPAs are housed in a boron nitride nozzle extension. The forcing Strouhal number is ranged from 0.07 to 2.62 for azimuthal modes of 0-3, ±1, ±2, and ±4. In the perfectly-expanded jet, the most effective forcing is obtained at m = ±1 and the jet spreading is significantly enhanced at a forcing Strouhal number of about 0.3 at this mode. For the perfectly-expanded jet, the effects of forcing on the jet development and structure formation are very similar to those observed in a M_J = 0.9 subsonic jet, which has been investigated previously. However, the generated structures in the imperfectly-expanded jets are less energetic due to the competition for energy between the perturbations seeded by the actuators and naturally existing perturbations amplified by the flow and acoustic feedback loop. As a result of this phenomenon, in addition to the fact that the jet mixing is already enhanced by the feedback loop, the mixing enhancement due to the control in the imperfectly-expanded jets is less significant.

1. INTRODUCTION

Many researchers have worked on jet flow control to enhance mixing and/or reduce noise. Most of the earlier jet flow control was done in low-speed and low Reynolds number flows. In such flows, acoustic drivers were successfully used since the flow momentum and associated flow characteristic frequency are low. However, the acoustic driver does not have sufficient bandwidth and amplitude in high-speed and high Reynolds number flows, since characteristic flow frequency and flow momentum increase as the jet speed and Reynolds number rise.

Stated simply, the most successful manipulation of the jet flow is related to controlling the jet characteristic instabilities. There are two major instability modes in a jet: the initial shear layer instability and the jet column instability. These modes are based on two length scales in a free jet: the initial boundary layer momentum thickness (θ) at the nozzle exit and the nozzle exit diameter (D) for a circular nozzle or the nozzle exit height (h) for a rectangular nozzle. The initial shear layer instability frequency is scaled with the momentum thickness (θ) at the nozzle exit. The jet column instability or the jet preferred mode is the instability around the end and downstream of the potential core, and its frequency is scaled with the nozzle exit diameter (D) or height (h). The corresponding Strouhal numbers are St_θ (= $f\theta/U_j$) and St_D (= fD/U_j) for initial shear layer instability and jet column mode, respectively. The f and U_j are instability wave frequency and the jet exit velocity, respectively.

[1]Corresponding author, Samimy.1@osu.edu

The shear layer of an unforced jet in the vicinity of the nozzle exit is very thin so that its behavior is very similar to that in a planar shear layer, since curvature effects are negligible. The mixing layer near the exit of the jet is referred as initial shear layer. In the initial shear layer, the maximum amplification of disturbances seems to occur around the Strouhal number ($St_\theta=f\theta/U_j$) of 0.012 in unforced jets [Zaman and Hussain 1981], while the maximum amplification rate of disturbances occur around St_θ=0.017 [Freymuth 1966, Michalke 1965] in forced jets. The input excitation amplitude required to control this instability in low-speed flows is very small and linear instability analysis has been used extensively to explore various aspects of this instability [Michalke 1965]. When the initial shear layer is forced, the increased amplification rate leads to earlier saturation of amplification and breakdown of amplified instability waves/vortices into smaller scales so that the amplification of instability is smaller than that in unperturbed jets [Zaman and Hussain 1981]. Thus, turbulence intensity in the downstream region can be reduced when the initial shear layer is forced at St_θ = 0.017. However, the growth of instability at St_θ = 0.012 leads to the large scale structures in the shear layer of the jet, which are responsible for the entrainment of ambient air into the jet and gross mixing with the jet fluid.

The maximum amplification of the jet column instability occurs over a wide range of St_D from 0.2 to 0.6 [Cho et al. 1998; Crow and Champagne 1971; Gutmark and Ho 1983; Ho and Huerre 1984], depending heavily upon the experimental facility. This is presumably due to the variations in the naturally occurring disturbances in the facilities. The jet column mode can be excited directly by forcing the mode with high enough amplitude [Cho et al. 1998].

In addition to the two instability modes discussed above, there is azimuthal mode instability in a circular jet. The jet column instability is unstable to azimuthal or helical modes [Cohen & Wygnanski 1987]. In a Mach 0.9 subsonic jet, the effects of azimuthal modes were maximum near the jet column instability frequency [Kim et al. 2007 & 2009].

The initial shear layer instability and the jet column mode can be coupled when the momentum thickness at the nozzle exit is relatively thick [Ho and Hsiao 1983]. The coupling occurs through an integer number (usually 3 or 4) of pairings of relatively small structures in the initial shear layer. Kibens [1980] also observed a coupling of these two modes in a forced jet with an acoustic driver. However, the Strouhal number along the lip-line of the jet was not stepwise, but smoothly changed. This suggests that the pairing did not occur in an orderly manner so that the coupling of the two modes perhaps did not happen [Ginevsky, et al. 2004]. Based on earlier results in Mach 0.9 subsonic [Kim et al. 2009] and Mach 1.3 supersonic [Samimy et al. 2007b] jets, it seems that the jet column mode is directly forced by the actuators.

As the Reynolds number of a flow increases, the actuator needs to have higher bandwidth and higher amplitude since the corresponding frequency of instability modes and also flow momentum increase. To meet this requirement, a plasma based actuation system was developed at the Gas Dynamics and Turbulence Laboratory (GDTL). This system, known as Localized Arc Filament Plasma Actuators (LAFPAs), can provide excitation signals of high amplitude and high frequency for high-speed and high Reynolds number flow control [Samimy et al. 2007a]. The ideally expanded Mach 1.3 jet was effectively forced at the jet column mode by LAFPAs [Samimy et al. 2007b]. While the jet responded to the actuation over a large St_D and various azimuthal modes (axisymmetric, helical, and flapping), the maximum spreading occurred around St_D of 0.3 for the flapping mode. The duty cycle of the actuation also played a significant role and the best result was observed at a low value of 5 – 10%.

When the LAFPAs were used in a high subsonic jet of Mach 0.9, the jet noise was reduced at a forcing Strouhal number around 1.1 or higher [Samimy et al. 2007a]. The level of noise reduction depended on both forcing frequency and azimuthal mode. The LAFPAs were also used in a 7.5 times larger nozzle at NASA with an exit diameter of 19.05 cm to explore their scale-up capabilities [Samimy et al. 2006]. This scalability test showed that the effects of forcing in a lager jet were similar at Mach 0.5. However, the actuators appeared to lack control authority at higher Mach numbers, as only 8 actuators, which had been designed for much smaller jet at GDTL, were used. In an axisymmetric Mach 0.9 jet, the effects of forcing frequency and mode were explained by using vortex dynamics [Kim et al. 2007, 2009]. The pattern of structures, as well as their spacing and size, were strongly dependant on the forcing frequency and mode. The jet mean flow and turbulence developments were well explained by the dynamics of the generated structures.

In the present research, the effects of forcing frequency and modes will be further explored in a perfectly-expanded jet of design Mach number 1.3 and two imperfectly-expanded jets. Similar to what was done in Mach 0.9 jet [Kim et al. 2007], the generated vortices will be visualized, and their roles in the jet mean and turbulence characteristics will be investigated.

2. FACILITY AND TECHNIQUES

All the experiments were conducted at the Gas Dynamics and Turbulence Laboratory at the Ohio State University. The compressed air, which is filtered and dried, is stored in two cylindrical tanks with a capacity of 43 m^3 up to 16 MPa. The compressed air is supplied to the storage tank and then to the stagnation chamber of the jet by three five-stage compressors. The air is then discharged through the converging-diverging nozzle of 2.54 cm exit diameter, designed by the method of characteristics to obtain shock-free uniform exit velocity. The nozzle design Mach number is 1.3. At the end of the nozzle, a boron nitride nozzle extension is attached to house eight plasma actuators, uniformly distributed in azimuthal direction (Fig. 1). Each actuator is composed of two tungsten pin electrodes with a diameter of 1 mm. The center-to-center distance of two electrodes is about 4 mm at the tip. All electrodes are placed 1 mm upstream of the extension exit within a ring groove, measuring 1 mm wide and 0.5 mm deep, to prevent the plasma from being blown off. As shown in Figure 1, the electrodes are installed radially and the tip of each electrode is flush-mounded to the inner surface of the nozzle extension. A more detailed description of actuators is in Utkin et al. [2007] and Kastner et al. [2009]. Investigation is conducted at three fully-expanded jet Mach numbers (M_J) of 1.2 (over-expanded), 1.3 (perfectly-expanded), and 1.4 (under-expanded). The jet exit centerline velocity is about 380 m/s, and the Reynolds number based on the nozzle exit diameter ranges from1.1x10^6 to 1.4x10^6.

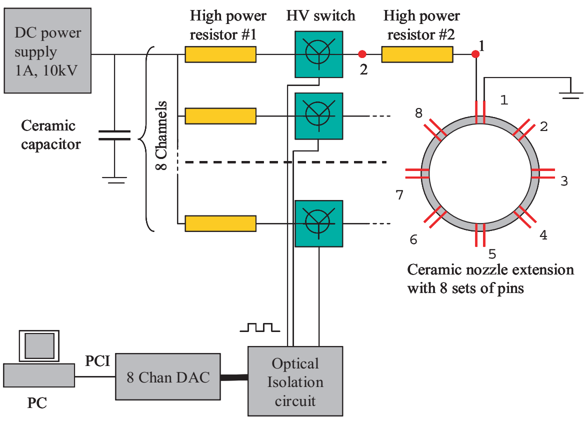

Figure 1. Schematic of the in-house fabricated 8-channel plasma generator.

The jet velocity field is measured by a LaVision PIV system using either one or two camera with 2048x2048 pixel resolution. A Spectra Physics Model SP-400 dual-head Nd:YAG laser is used for the light source. The cameras and laser are synchronized by a timing unit housed in a dual-processor PC. The setup for the PIV is depicted in Figure 2. The spatial resolution of the velocity vectors depends on the field of view, and the number of pixels used. For the most of streamwise velocity filed measurements, the spatial resolution is about 2.5 mm.

The jet plume is seeded with Di-Ethyl-Hexyl-Sebacat (DEHS) liquid droplets atomized by a four jet LaVision atomizer. A 38.1 cm (15”) duct is placed upstream of the jet exit to generate a co-flow. The co-flow is generated by channeling part of the entrained air into the jet through the duct without using any fans or blowers. The co-flow is seeded by a fogger to avoid spurious velocity vectors in the entrained air region. The average droplet size is about 0.25 and 0.7 μm for the jet flow and co-flow, respectively. The turbulence statistics were converged using 600 to 650 image pairs [Kim et al. 2007, 2009]. Thus, about 700 image pairs are used for all the statistics reported in this paper. The uncertainty in the PIV measurements is related to many parameters such as the particle size and density, and turbulence scales of interest. Within 5% deviation from the actual turbulence intensity, the seeded particles trace the flow up to 20 and 70 kHz of turbulence fluctuations frequency for 0.7 and 0.25 μm particles, respectively [Melling 1997]. Based on this calculation, the uncertainty of turbulence intensity is about 5% up to Strouhal number of 1.33. However, the uncertainty level for the mean and turbulence statistics was within ±3% and ±15%, respectively, based on the repeatability measurements for the baseline jet. In the shock-containing imperfectly expanded jets, the particles lag behind the actual flow speed in regions near the shocks. Melling [1997] showed that for a 0.25 μm particle passing through an oblique shock wave (upstream and downstream Mach numbers are 1.5 and 1.15, respectively), it needed about 0.5 mm to reach 95% of the downstream velocity. In the present research, the shock is not quite strong so that an estimated distance required for the particle to reach 95% of the downstream velocity is about 0.2 mm. Thus, the uncertainty of the present PIV measurements is as specified earlier in most parts of the flow field measured.

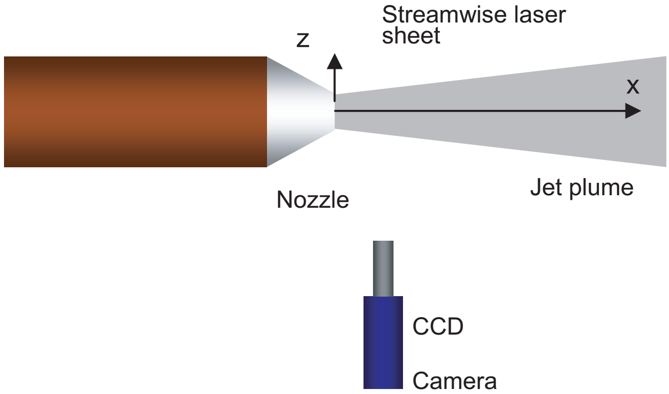

Figure 2. Schematic of the jet and the optical diagnostics set up at GDTL. Y-coordinate is normal to the plane.

The plasma generating system, shown in Figure 1, has two high voltage Glassman DC power supplies, with output of 10 kV and 1 Ampere. Each power supply can drive four actuators simultaneously, and thus up to eight actuators can be operated at the same time. Each actuator is controlled independently by a Behlke high voltage transistor switch. A National Instrument (NI) analog board attached to a PC is used to generate eight independent, continuous pulse trains to control the transistor switches. Details of the plasma system are provided in Utkin et al. [2007] and in Samimy et al. [2007b].

The forcing frequency, duty cycle, and azimuthal mode are controlled through LabView, NI software. The available azimuthal modes with eight actuators are m = 0-3, ±1, ±2, and ±4, where m indicates azimuthal mode. A detailed description of the azimuthal modes is in Kim et al. [2009]. Although experiments are conducted for all these modes, more extensive results for m = 0, 1, and ±1 will be presented since these modes were representative in Mach 0.9 jets [Kim et al. 2007, 2009]. The forcing Strouhal number ($St_{DF} = f_F D/U_j$, f_F is forcing frequency) ranges from 0.07 to 2.62, covering the jet column mode instability and the lower end range of the initial shear layer instability. The jet exit velocity is used in calculating the forcing Strouhal numbers for all jet Mach numbers, and its value varies slightly due to the variation of the stagnation temperature.

3. RESULTS

The performance of the plasma actuators will be evaluated by PIV measurements. The centerline Mach number decay and the jet width (δ), defined by the full width at half maximum (FWHM) of the streamwise velocity, will be used for overall performance evaluation. The spacing and convection velocity of generated large-scale structures will be obtained from spatial cross-correlation and these will be used for conditional averaging of PIV images. The large-scale structures will be visualized by using conditionally-averaged Galilean velocity fields (the coordinate systems are moving with the convective velocity of large-scale structures). From this information about large-scale structure, the role of the generated structures in the jet development will be discussed extensively.

3.1 Effects of Forcing Strouhal number on Overall Jet Mixing

The results for Mach 0.9 subsonic [Kim et al. 2007, 2009] and perfectly-expanded Mach 1.3 supersonic [Samimy et al. 2007b] jets showed that the forcing is most effective at m = ±1. Thus, the results at m = ±1 are used for the evaluation of the effects of St_{DF} numbers on the jet spreading. Average streamwise velocity contours for m = ±1 are shown in Figure 3 for three fully-expanded jet Mach numbers of 1.2 (over-expanded), 1.3 (perfectly-expanded), and 1.4 (underexpanded). The streamwise velocity is scaled from -40 m/s to the maximum for each Mach number. The maximum jet velocity is about 360, 380, and 420 m/s for M_J = 1.2, 1.3, and 1.4, respectively. Thus, no information can be gained from a one-to-one comparison of the colors in plots of differing Mach number.

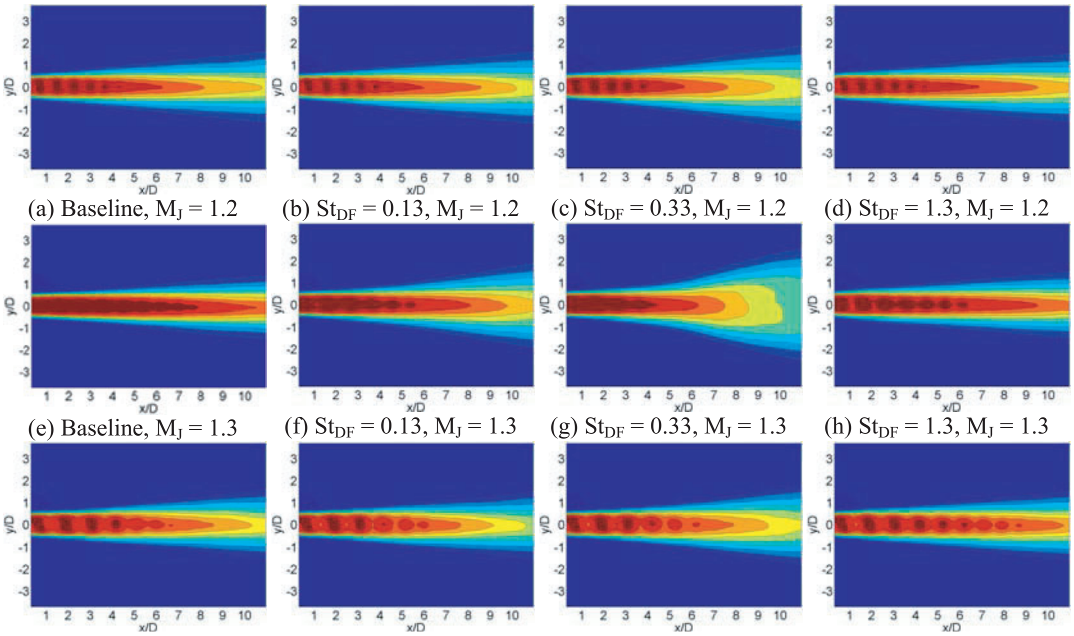

(a) Baseline, $M_J = 1.2$ (b) $St_{DF} = 0.13$, $M_J = 1.2$ (c) $St_{DF} = 0.33$, $M_J = 1.2$ (d) $St_{DF} = 1.3$, $M_J = 1.2$

(e) Baseline, $M_J = 1.3$ (f) $St_{DF} = 0.13$, $M_J = 1.3$ (g) $St_{DF} = 0.33$, $M_J = 1.3$ (h) $St_{DF} = 1.3$, $M_J = 1.3$

(i) Baseline, $M_J = 1.4$ (j) $St_{DF} = 0.13$, $M_J = 1.4$ (k) $St_{DF} = 0.27$, $M_J = 1.4$ (l) $St_{DF} = 1.3$, $M_J = 1.4$

Figure 3. Average streamwise velocity contours for various St_{DF} numbers at three jet Mach numbers. The maximum velocity of the jet is about 360, 380, and 420 m/s for Mach = 1.2, 1.3, and 1.4 jets, respectively.

The baseline/unforced jets show that the jet spreading is increased at the off-design jets of $M_J = 1.2$ and 1.4. The enhanced spreading is due to the feedback loop sustained by upstreamtraveling acoustic waves and downstream traveling large-scale structures/hydrodynamic waves in the jet shear layers that interact with the shock waves generating the acoustic waves. A strong tone is also generated by the feedback loop in all three cases, as shown in Figure 4. For the imperfectly-expanded jets, the broadband shock associated noise (broad humps in the spectra) is significantly increased. However, the shock associated broad noise is not significant in the perfectly expanded jet (Figure 4b). The shock cell patterns are clearly seen in the average streamwise velocity contours for the imperfectly-expanded jet (Figures 3a & i). Thus, the shock strength is less in the perfectly-expanded jet than in the imperfectly-expanded jet. This can be more clearly observed in the centerline Mach number to be presented later.

For the over-expanded jet ($M_J = 1.2$), the effect of forcing is not apparent at a low St_{DF} of 0.13. The maximum spreading occurs at a St_{DF} of 0.33 (Fig, 3c), but the enhancement of jet spreading is moderate. At a higher St_{DF} of 1.3 (Figure 3d), it appears that the jet spreading is even suppressed. The contours for the under-expanded jet (Figures 3i-l) show that the trend of jet spreading with St_{DF} is very similar to that for the over-expanded jet. For this flow regime, the maximum spreading is at a slightly low St_{DF} of 0.27 (Figure 3k). As will be further discussed, the forcing is less effective in the imperfectly-expanded jets when compared to the perfectly-expanded Mach 1.3 jet.

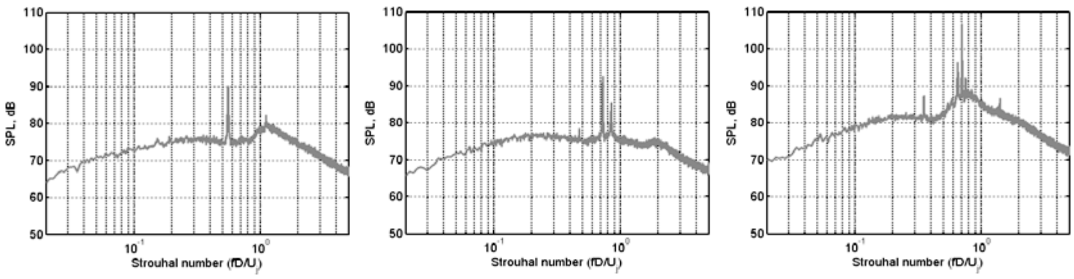

(a) $M_J = 1.2$ (b) $M_J = 1.3$ (c) $M_J = 1.4$

Figure 4. Average spectra at $M_J = 1.2$, 1.3 and 1.4, measured at 90° relative to the jet centerline.

For the perfectly expanded jet (M_J = 1.3), the jet responds to the forcing in a wide range of St_{DF}'s. At a low St_{DF} of 0.13, the jet spreading is significantly enhanced, contrary to the imperfectly-expanded cases. The maximum spreading is observed at a St_{DF} of 0.33 (Figure 3g) and the enhancement in the jet spreading is dramatic. At a high St_{DF} of 1.3, the velocity contour is very similar to that of the baseline, implying that forcing is not effective at high St_{DF}'s. The trend observed at the perfectly-expanded Mach 1.3 supersonic jet is very similar to what was observed in a subsonic Mach 0.9 jet [Kim et al. 2007, 2009].

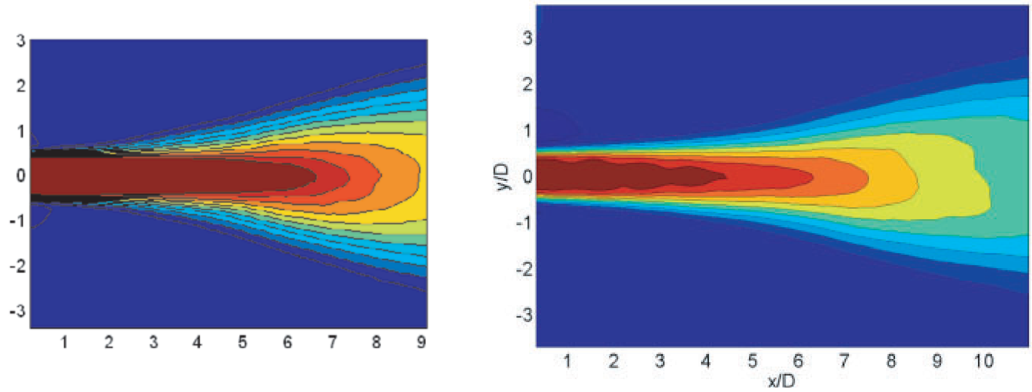

(a) M_J = 0.9 [Kim et al. 2009] (b) M_J = 1.3

Figure 5. Average velocity contours in the flapping plane at m = ±1 and $St_{DF} \approx 0.3$. The scale is about the same, but the spans in streamwise and cross-streamwise directions are different.

Figure 5 shows the streamwise velocity contours measured by the PIV system for Mach 0.9 and 1.3 jets, respectively, at a St_{DF} of about 0.3 and at m = ±1. Note that the color map is not the same – the same color does not represent the same speed. The jet exit velocity is about 280 and 380 m/s for M_J = 0.9 and 1.3, respectively. In both jets, the actuators have control authority and the enhancement of mixing/spreading (spreading from here on) is about the same. As will be further discussed in a later section, the nature and role of generated structures in the jet development are also about the same.

The effects of forcing Strouhal number will be more extensively presented by examining jet width and jet centerline Mach numbers. For M_J = 1.3, the jet width development at m = ±1 is shown in Figure 6 at various St_{DF}'s. The jet width in Figures 6a&b is on the flapping plane, which shows the effects of forcing Strouhal number. The jet width on the non-flapping plane (not shown here) does not show any significant spreading. Thus, the cross-section of the jet plume is elliptic at this forcing mode. An equivalent jet width, defined as the geometric average of the jet width in the flapping and non-flapping planes (square root of the multiplication of two jet widths), is shown in Figures 6c&d. One could then compare this jet width with those of other modes, which are axisymmetric in the average sense. As in the M_J = 0.9 subsonic jet [Kim et al. 2009], the jet plume spreading was significantly enhanced by forcing. As the St_{DF} number is increased, the spreading also increases up to $St_{DF} \approx 0.3$ as shown in Figures 6a & c. When the St_{DF} number is further increased, the jet spreading is decreased as shown in Figures 6b & d and more visually in Figure 3h. Thus, the enhancement of the jet width is greatest at $St_{DF} \approx 0.3$. At high St_{DF}'s greater than 1.31, the jet width development is about the same as that of the baseline as can be seen also in Figures 3e&h. The trend of jet spreading with St_{DF}'s is more readily seen in Figure 7, showing the jet widths at x/D = 10 for m = ±1. In the figure, the jet width for the forced cases is normalized by that for the baseline. The normalized jet width increases rapidly at St_{DF}'s approaching 0.33. For St_{DF}'s greater than 0.33, the normalized width decreased with increasing St_{DF}'s as was seen in Figures 3 and 6. These results show that the performance of the actuators is about the same in both Mach 0.9 subsonic and perfectly-expanded Mach 1.3 jets.

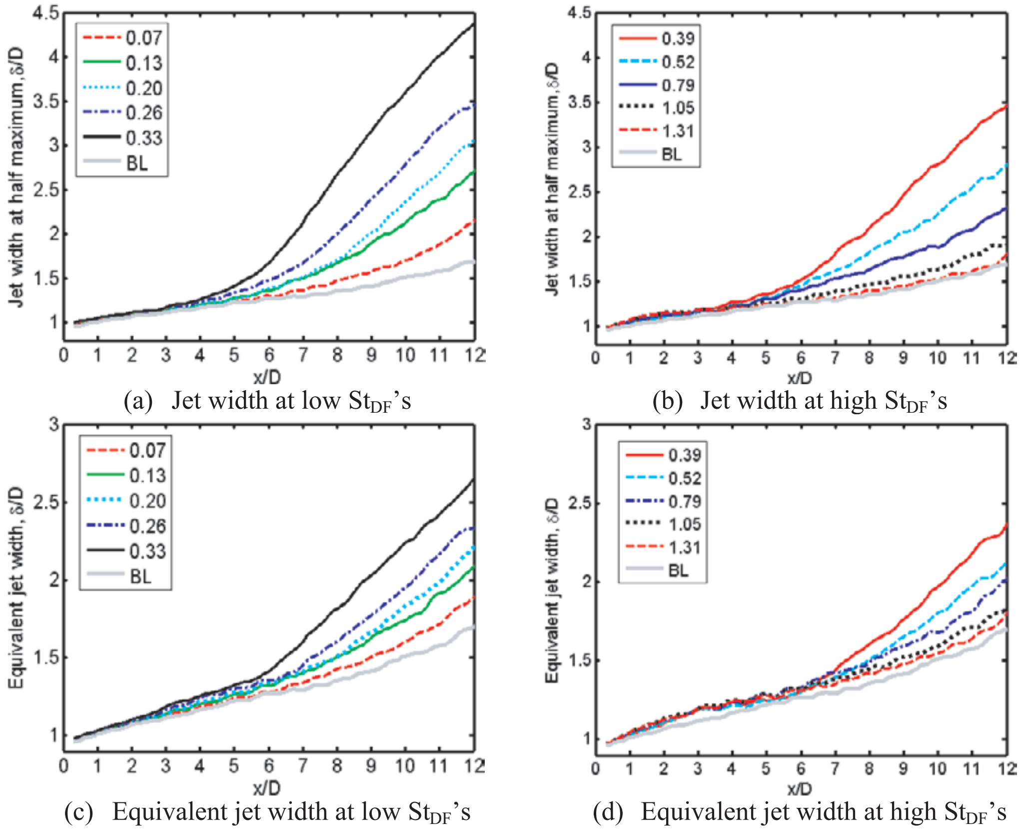

(a) Jet width at low St_{DF}'s (b) Jet width at high St_{DF}'s

(c) Equivalent jet width at low St_{DF}'s (d) Equivalent jet width at high St_{DF}'s

Figure 6. Jet width development at m = ±1 for various St_{DF} numbers.

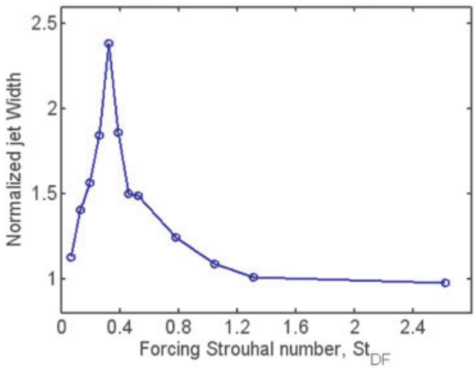

Figure 7. Normalized jet widths on the flapping plane at x/D = 10 for m = ±1. The jet width at each St_{DF} number was normalized by that for the baseline.

For the imperfectly-expanded Mach 1.2 & 1.4 jets, the jet width development with downstream location at m = ±1 is shown in Figure 8. In both jets, the jet width increases at low St_{DF}'s less than about 0.3. The enhancement of jet spreading is maximum at St_{DF} numbers 0.33 and 0.26 for M_J =1.2 and 1.4, respectively. The jet width x/D = 10 shows a dip and secondary peak at high St_{DF} numbers when the St_{DF} number is increased further from the maximum (Figure 8c), which was not seen in the perfectly-expanded jet (Figure 7). For some other azimuthal modes (not shown here), the normalized jet width is undulating with St_{DF} numbers. This difference in jet width trend is possibly due to the interaction of the forced and naturally amplified (by the feedback loop) structures as will be further discussed later. At St_{DF}'s greater than 1.0, the jet width is reduced by forcing as was also observed in the velocity contours in Figure 3. The overall enhancement of jet spreading is not as significant as in the perfectly-expanded jets. It seems that the reduction in jet spreading at high St_{DF} numbers and overall spreading is also associated with the interaction of the forced and naturally occurring structures.

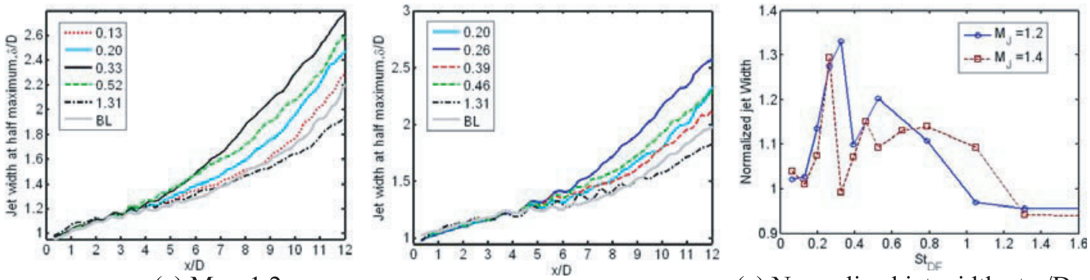

(a) $M_J = 1.2$ (b) $M_J = 1.4$ (c) Normalized jet width at x/D =10

Figure 8. Jet width development on the flapping plane at m = ±1 for the imperfectly-expanded jets.

For other azimuthal modes, the optimal St_{DF} numbers are selected from the normalized jet width at x/D = 10 and are shown in Table 1. For the most cases, the optimal St_{DF} number is about 0.3. Exceptionally low numbers are seen at 0.13 for M_J = 1.3 & m = 3 and 0.06 for M_J = 1.4 & m = 2. For other cases, the numbers are within 0.2-0.6 range, found in the literature.

Table 1. Optimal St_{DF} numbers, showing maximum jet spreading at each azimuthal mode.

Azimuthal mode	$M_J = 1.2$	$M_J = 1.3$	$M_J = 1.4$
m = 0	0.52	0.52	0.33
m = 1	0.26	0.39	0.26
m = 2	0.26	0.33	0.06
m = 3	0.20	0.13	0.26
m = ±1	0.33	0.33	0.26
m = ±2	0.52	0.33	0.46

3.2 Effects of azimuthal modes

3.2.1 Perfectly-expanded jet

The results presented in the earlier section showed the effects of St_{DF} numbers at m = ±1. In this section, the effects of azimuthal modes will be discussed by using optimal cases; those that show the most jet spreading. For the perfectly-expanded jet, the average streamwise velocity contours at the optimal St_{DF} numbers, listed on Table 1, are shown in Figure 9. Also, the profiles of the centerline Mach number and jet width are shown in Figure 10 for the optimal St_{DF}'s. Note that an equivalent jet width is used only for m ±1 since the jet cross-section is elliptic for this mode. The streamwise velocity contours and centerline Mach number show that the jet potential core length is shortened significantly for m = 1 and ±1, and moderately for the other modes. The potential core length is reduced from 7 nozzle diameters in the baseline jet to 4 (for m = 1 & ±1) and 5.5 (for the rest of modes). Although both the potential core length and centerline Mach number are indirect measures for the jet growth/spreading, the trend observed in Figures 9 and 10a is very similar to what is seen in the jet width, a direct measure for the spreading. There is a moderate undulation in the centerline Mach number due to weak shock cells. Although the diverging section of the nozzle was designed by the method of characteristics, the occurrence of weak shocks is unavoidable with a thick lipped nozzle. For all azimuthal modes, the centerline Mach number decay is enhanced by forcing. The results in Figures 9 and 10 show that the most effective forcing is at m = ±1. At this mode, a dramatic enhancement in jet spreading is manifested in accelerated centerline Mach number decay and enhanced jet width. Additionally, the spreading at m = 1 is substantially improved. For the rest of the azimuthal modes, the enhancement in jet spreading is moderate.

The results in the perfectly-expanded Mach 1.3 jet are largely similar to those in Mach 0.9 subsonic jets [Kim et al. 2009]. However, the jet growth at m = ±2 is significantly reduced compared to those in Mach 0.9 jets. In the Mach 0.9 jet, the increase in centerline Mach number decay was similar for both m = ±2 and m = ±1 cases. In the perfectly-expanded Mach 1.3 jet, the jet growth at m = ±2 is about the same as the moderately effective group of modes (m = 0, & 2-3). At this point, it is not clear why the performance at m = ±2 was reduced in Mach 1.3 jets. Another difference is the growth in the initial shear layer. In Mach 0.9 subsonic jets, a significant enhancement in jet width in the initial shear layer was seen for many azimuthal modes at a relatively high St_{DF} of about 1.0 [Kim et al. 2007, 2009]. For the perfectly-expanded Mach 1.3 jet, the enhancement in jet width in the initial shear layer is only seen at m = 3 (shown in Figure 11) and is not as significant as in the subsonic counterpart. The increased jet width upstream of the end of potential core is thought to be due to growths of the structures generated by forcing.

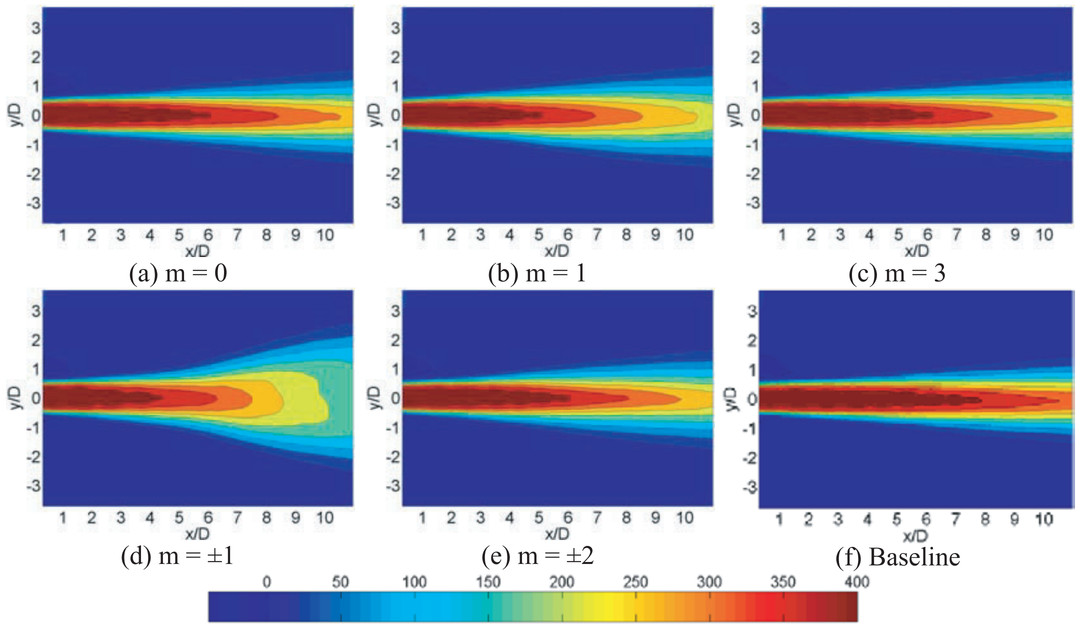

Figure 9. Average streamwise velocity contours at the optimal St_{DF}'s, listed in Table 1, for each azimuthal mode.

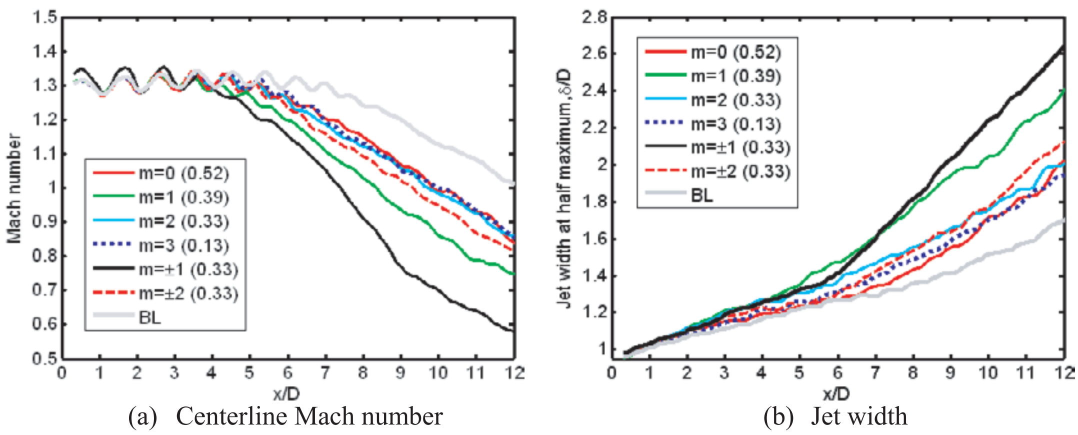

Figure 10. Comparison of the centerline Mach number and jet width at M_J = 1.3. For m = ±1, the jet width is the equivalent width. The forcing Strouhal number is shown in the legend of each figure.

3.2.2 Imperfectly-expanded jets

The centerline Mach number and jet width development for three modes of m = 0, 1, and ±1 are compared to show the effects of azimuthal mode in the over-expanded jets (Figure 12). In this figure, the St_{DF} number for each azimuthal mode is selected for the maximum jet spreading as listed in Table 1. In the over-expanded M_J = 1.2 jet, the centerline Mach number is a better measure for the overall jet spreading since no measurement is done on the non-flapping plane for the m = ±1 case. Neither the potential core length, obtained from Figure 12a, nor the centerline Mach number decay rate beyond the end of potential core is significantly altered by forcing. The ineffectiveness of forcing in the over-expanded jet is also manifested in the average streamwise velocity contours shown in Figure 13. The shock cell patterns in the potential core region and jet growth are barely changed by forcing. However,

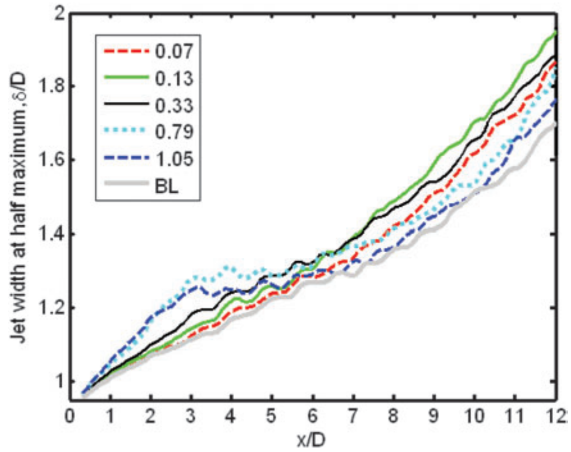

Figure 11. Jet width development along the streamwise direction at m = 3.

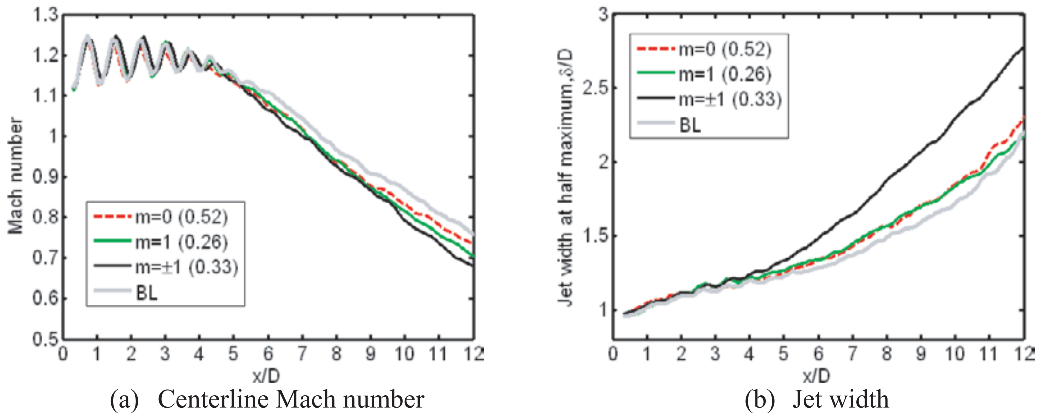

Figure 12. Comparison of the centerline Mach number and jet width at M_J = 1.2. The jet width for m = ±1 is on the flapping mode. The forcing Strouhal number is 0.52, 0.26, and 0.33 for m = 0, 1, and ±1, respectively.

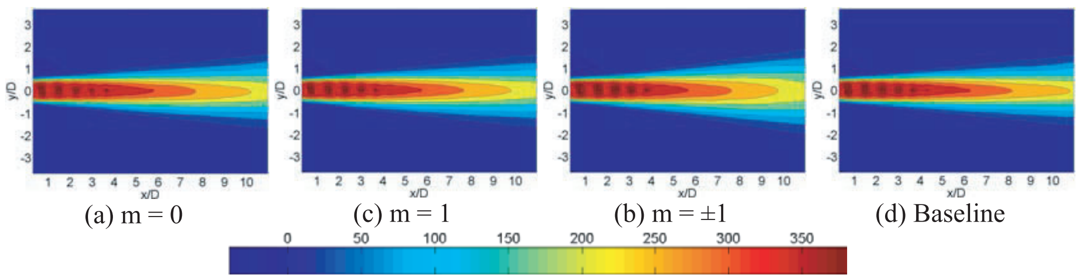

Figure 13. Average streamwise velocity contours in the over-expanded jet (M_J = 1.2).

the jet width on the flapping plane at m = ±1 shows a notable increase, suggesting that large-scale structures are generated. However, it seems that the generated large-scale structures lack the strength to significantly excite the shock containing jet and so do not increase mixing. This will to be discussed further later. For the other modes not presented here, the spreading is about the same as that for m = 0 or 1. These results show that the forcing in the over-expanded jet is not as effective as in the perfectly-expanded jet.

For the under-expanded M_J = 1.4 jet, the centerline Mach number and jet width are shown in Figure 14 for m = 0, 1, and ±1. For the other modes not shown here, the centerline Mach number and jet width are very similar to that for m = 1 and m = 0, respectively. Again, in this figure, the forcing Strouhal number for each azimuthal mode is selected for the maximum jet spreading as listed in Table 1. The centerline Mach number undulates between 1.3 and 1.5 due to periodic shock cell structures in the jet. The jet potential core length and centerline Mach number decay are not significantly changed by forcing, as in the over-expanded jet. The jet width is increased slightly by forcing, but the increase is not as significant as in $M_J = 0.9$ subsonic [Kim et al. 2007, 2009] or ideally expanded $M_J = 1.3$ jets. The jet width enhancement at m = ±1 seems significant, but note that the non-flapping plane width, which would be very close to that for the baseline, is not taken into account. The equivalent jet width, geometric average of the jet width on the flapping and non-flapping planes, is expected to be very close to that for the m = 0. This explains why the centerline Mach number decays for m = 1 and ±1 are very close to each other as seen in Figure 14a. The reduced jet spreading over the baseline jet is partially due to enhanced mixing in the baseline/unforced jet as discussed earlier (Figures 3a,e,&i).

In $M_J = 1.4$ jets, the centerline Mach number decay is slightly suppressed for all azimuthal modes except for m = ±1, as shown in Figure 14a. For m = 0, the centerline Mach number decay is significantly reduced and the jet width development is almost the same as the baseline. In the Mach 0.9 subsonic jets, it was shown that vortex rings were generated at m = 0, and that the centerline velocity decay and jet spreading were reduced due to self induction and axisymmetric nature of the vortex ring [Kim et al. 2007 & 2009].

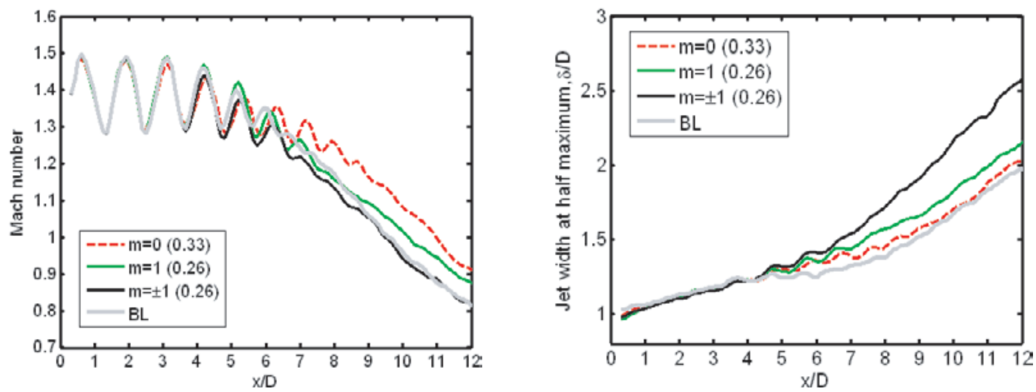

(a) Centerline Mach number (b) Jet width

Figure 14. Comparison of centerline Mach number and jet width at $M_J = 1.4$. The jet width for m = ±1 is on the flapping mode. The number in the parentheses indicates the forcing Strouhal number for each azimuthal mode.

3.3 Effects of Forcing on Turbulence

This section examines the development of jet centerline two-dimensional turbulent kinetic energy (TKE henceforth), as only a two-component PIV system was utilized. The effects of forcing Strouhal number at m = ±1 on TKE is shown in Figure 15 in the perfectly-expanded jet. The TKE level is significantly increased at a St_{DF} number near of 0.3, but its level is close to that for the baseline at low (not shown here) and high St_{DF} numbers (1.31, for an example). For the St_{DF} of 0.33 which showed maximum jet growth, the TKE level saturates at x/D = 8 and then slowly decays. For other forced cases, the TKE level increases almost monotonically without showing any saturation in the entire streamwise measurement span.

Figure 16 shows the effects of azimuthal modes for three flow regimes of $M_J = 1.2$, 1.3, and 1.4. The cases shown in the figure are for forcing Strouhal numbers that achieved maximum spreading for each mode, listed in Table 1. The forcing Strouhal numbers for each mode correspond to those shown Figures 10, 12, and 14, respectively. For $M_J = 1.3$, TKE is significantly increased for all forcing modes. The TKE saturates at x/D = 8.5 and 10.5 for m = ±1 and 1, respectively. This suggests that the earlier saturation of TKE indicates increased jet growth/spreading. As in a $M_J = 0.9$ subsonic jet, the TKE is still on the rise for m = 0. This is due to self-induction by vortex rings and the symmetric nature of the generated structures in this mode [Kim et al. 2007 & 2009]. This behavior can be explained by the dynamics of the generated structures and a more detailed discussion will be presented later.

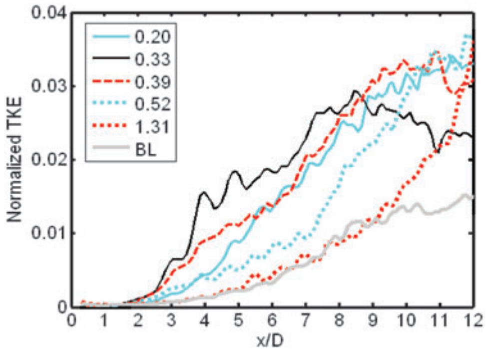

Figure 15. Turbulent kinetic energy development at m = ±1 in the perfectly-expanded jet.

For imperfectly-expanded jets of M_J = 1.2 and 1.4, it appeared that centerline TKE is not significantly altered by forcing as seen in Figure 16b &c. This is partially due to increased TKE level in the unforced baseline jets and also the presence of relatively strong shock/expansion train. As was discussed earlier, when the jet operates in imperfectly-expanded regime, a screech tone is generated by a feedback loop between the hydrodynamic and acoustic waves (Figure 4), and largescale structures are amplified due to this feedback loop resulting in the increase in TKE. If the large-scale structures are suppressed, TKE would be reduced by forcing. This was observed when the jet was forced at high St_{DF}'s (not shown here).

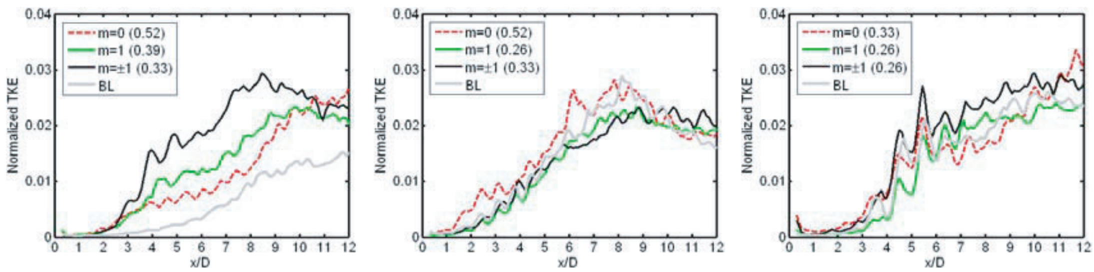

(a) M_J = 1.3 (b) M_J = 1.2 (c) M_J = 1.4

Figure 16. Two-dimensional turbulent kinetic energy development for three azimuthal modes m = 0, 1, and ±1.

3.4 Large-Scale Structures and their role in the Jet Development

Large-scale structures are visualized by using conditionally averaged Galilean velocity field. In the Galilean velocity field, the reference frame moves with the convection velocity of large-scale structures in the flow. Thus, the large-scale structures are stationary in this frame, and they are identified if the streamlines show closed or spiral shapes [Kline and Robinson 1990, Robinson et al. 1989]. A more detailed procedure for visualizing large-scale structures is in Kim et al. [2007 & 2009].

3.4.1 Perfectly-Expanded Jet (M_J = 1.3)

Large-scale structures for excitation with m = ±1 at various Strouhal numbers in the M_J = 1.3 jet are shown Figure 17. The relative magnitude of the streamwise velocity is represented by color: red and blue indicate fast and slow speeds, respectively. There is no common color map, valid for all images, since the reference frame moves at a different speed for each case. Large periodic structures are generated by forcing at a wide range of St_{DF}'s from 0.2 to 1.05. At St_{DF}'s outside of this range, there are no visible periodic structures in the shear layer as shown in Figure 17e, as an example.

At St_{DF} = 0.33, the generated structures are very robust and well organized. The generated structures are nearly circular in shape, penetrating into the jet centerline, and causing significant undulation in the jet plume. The potential core length is about four nozzle exit diameters as shown in Figure 10a. The potential core is significantly shortened by the entrainment of ambient air and penetration of energetic structures into the jet as seen in Figure 17b. Also, the jet spreading is significantly enhanced by the robust structures as shown in Figure 10b. The generated structures either decays completely and/or become very disorganized by x/D = 7 – no identifiable large structures are seen downstream of this

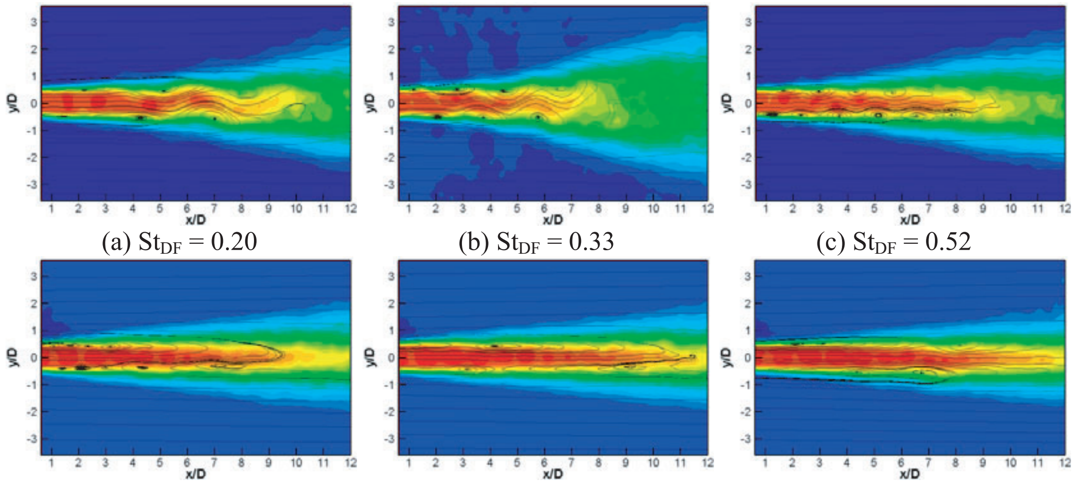

(a) $St_{DF} = 0.20$ (b) $St_{DF} = 0.33$ (c) $St_{DF} = 0.52$

(d) $St_{DF} = 1.05$ (e) $St_{DF} = 1.31$ (f) Baseline

Figure 17. Galilean streamlines superimposed on the streamwise velocity fields at m = ±1 in the $M_J = 1.3$ jet. The velocity fields were conditionally-averaged and the number of images used for the averaging was 30.

location. As shown in Figure 15, the TKE development is saturated at this location and this saturation location is related to the sudden decay of large-scale structures.

At a low St_{DF} number of 0.2, the generated large periodic structures appear to be nearly elliptical with a high aspect ratio aligned in the streamwise direction. This may be due to a limited growth of the structures in the spanwise direction when compared to that at $St_{DF} = 0.33$. Also, the interaction between the generated structures and the jet plume appears to be limited. The monotonic increase in TKE (Figure 15) up to x/D of 12 indicates that the interaction between structures is significantly less for this case. This can be inferred from a longer spatial lifetime of the generated structures at $St_{DF} = 0.2$ than at $St_{DF} = 0.33$. Some large structures are seen up to x/D = 10 at $St_{DF} = 0.2$ while all structures had decayed by x/D = 7 for $St_{DF} = 0.33$. As in $St_{DF} = 0.33$ case, the jet plume is undulating in the lateral direction due to the flapping action caused by the generated structures. However, the undulating motion is not as significant as in $St_{DF} = 0.33$ case due to the less energetic structures. As a result, the mixing enhancement is relatively less significant at this forcing Strouhal number.

At a moderate St_{DF} of 0.52, periodic large structures, with a reduced spacing, are generated. The interaction between generated structures seems minimal, which is inferred from the well-preserved periodic structures and their almost constant dimension up to x/D = 8. It seems that the jet plume undulates less since the generated structures are smaller than those at low St_{DF}'s. The reduced undulation of the jet plume suggests that the interaction between the generated structures and the jet plume is not significant when compared to that at low St_{DF}'s. The reduced TKE at this St_{DF} number, shown in Figure 15, also confirms that the interaction was decreased or limited at this moderate St_{DF}.

Interestingly, some periodic structures are observed even at a high St_{DF} number of 1.05 (Figure 17d). The generated structures are very small and closely spaced. It appears that these small structures decay faster than those at low St_{DF} numbers, but they are occasionally visible up to x/D = 8. Despite having a Reynolds number of about one million, these structures do not experience significant decay in the highly turbulent flow, as was also observed in Mach 0.9 subsonic jet [Kim et al. 2007 & 2009]. At a higher St_{DF} number of 1.3 (Figure 17e), no periodic structures are seen and the flow fields are very similar to that of the baseline (Figure 17f). In the baseline jet, there are some randomly spaced structures, but they are not energetic so that their effect on the jet plume is minimal. The structures observed in this $M_J = 1.3$ jet are very similar to what were seen in the $M_J = 0.9$ subsonic jet with a Reynolds number of about 0.7×10^6 [Kim et al. 2007, 2009].

Figure 18 shows the effects of St_{DF} number on the spacing (and also dimension) of the generated structures. The structure spacing is calculated from two-dimensional spatial correlation of 700 instantaneous velocity fields as detailed in Kim et al. [2007, 2009]. The spacing is inversely proportional to St_{DF} number as shown in Figure 18, and the streamwise dimension of the structures also shows the same trend as the structure spacing, as seen in Figure 17. The profiles for various azimuthal modes in Figure 18 are collapsed into a single curve using the following equation

$$\frac{\delta}{D} = \frac{a}{St_{DF}} + c \tag{1}$$

where a and c are constants. The figure shows that the structure spacing is strongly dependant on the St_{DF} number, and that effects of azimuthal modes are minimal. Also shown in the figure is that the perfectly-expanded jet responds to the forcing over a range of St_{DF} numbers from 0.2 to 1.3. This strong relation further confirms that the structures seen in Figure 17 were generated by the excitation/forcing rather than by any other means.

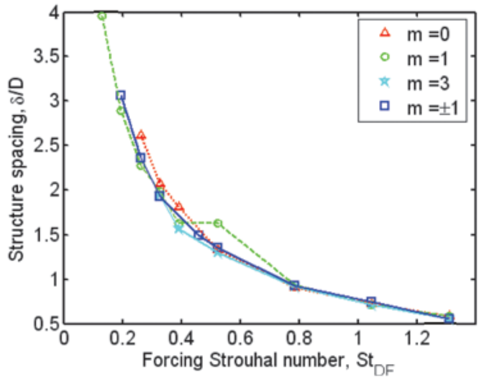

Figure 18. Spacing of the generated structures in M_J = 1.3 jets.

Figure 19 shows visualized large-scale structures for m = 0 and 1 at St_{DF} numbers showing the maximum spreading for each mode (Figure 10 and Table 1). For m = 0, the visualized structures are symmetric across the jet plume since they are vortex rings. The centerline streamwise velocity between a pair of vortical structures (actually inside a vortex ring) is faster due to self induction, but the flow between two neighboring vortex rings is slower due to the entrainment of slow moving ambient air [Kim et al. 2007, 2009]. Thus, the streamwise velocity along the jet centerline undulates, similar to what was observed in M_J = 0.9 subsonic jet [Kim et al. 2007]. As in the Mach 0.9 jet, the structures do not penetrate into the jet centerline due to the symmetric nature of the generated structures. Consequently, the interaction of large-scale structures and the jet plume is less destructive. As a result, the centerline Mach number decay is less than in that of any other mode as shown in Figure 10a. For m = 1, the pattern of the generated structures and jet plume undulation is very similar to that of m = ±1, but the structures seem less energetic. As a result, the enhancement in the jet width at this mode is less than that of m = ±1 (Figure 10b).

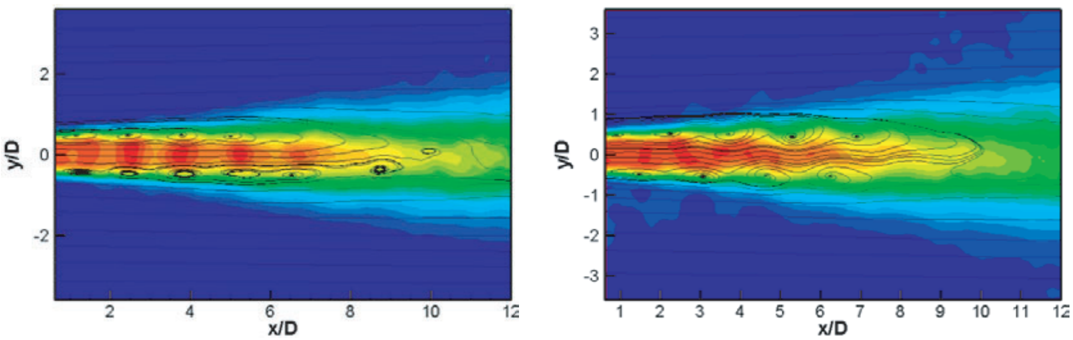

(a) m = 0 (St_{DF} = 0.52) (b) m = 1 (St_{DF} = 0.39)

Figure 19. Galilean streamlines superimposed on the conditionally-averaged streamwise velocity fields for the cases shown in Figure 10 or Table 1.

For other modes not shown here, the generated vortex pattern is very similar to that for m = 0 and 1 for even- and odd-numbered modes, respectively. For example, the vortex pattern of m = 2 is similar to that at m = 0, shown in Figure 19a. In Mach 0.9 subsonic jet, the streamwise component of turbulence was more amplified at even-numbers modes, while the cross-streamwise component was more amplified at odd-numbered modes. This is due to symmetric or asymmetric nature of the generated structures for even- or odd-numbered modes, respectively [Kim et al. 2007, 2009]. All these results show that the effects of forcing on the flow structures and jet development are very similar to what was observed in $M_J = 0.9$ subsonic jet [Kim et al. 2007]. Thus the discussion of the role of generated structures on the jet development presented in the subsonic case is still valid in this perfectly-expanded $M_J = 1.3$ supersonic jet.

3.4.2 Imperfectly-Expanded Jets (M_J = 1.2 and 1.4)

Flow visualizations were conducted at $M_J = 1.2$ and 1.4 to investigate whether the plasma actuators are effective in forcing flows containing a shock/expansion train. Some preliminary results presented in Samimy et al. [2007b, 2008] and the results discussed in earlier sections showed that the forcing is less effective in imperfectly-expanded jets (Figures 10, 12, & 14). The flow visualizations based on the condensed water particle showed that the jet responded to the forcing in a similar fashion as in perfectly-expanded $M_J = 1.3$ jet [Samimy et al. 2008]. However, it seemed that the jet did not respond to the actuation in the over-expanded $M_J = 1.2$ jet. The generated structures are visualized based using the Galilean velocity field to find an answer for the reduced effectiveness at the imperfectly-expanded jets.

Visualized large-scale structures are shown in Figure 20 for m = ±1 in the over-expanded $M_J = 1.2$ jet. These structures were also seen in flow visualizations in the earlier research [Samimy et al. 2008]. The generated structures seem as robust and energetic as in the perfectly-expanded jet (Figure 17). However, the enhancement in jet growth is not as significant as that in $M_J = 1.3$ jets as seen in Figure 12b. The spacing of the structures, the distance between two consecutive spiral shapes, are inversely proportional to St_{DF} numbers ranging from 0.2 to 1.1 as also shown in Figure 21. For m = 0 and 1, the jet responds in a narrower range of St_{DF} numbers from 0.3 to 0.8 when compared to the perfectly-expanded jet case shown in Figure 18. In the unforced/baseline jet, some periodic structures are observed, but they appear to be not well organized. However, an image acquired from the proper orthogonal decomposition (not shown here) showed that there are periodic structures in the baseline jet. The periodic structures in the proper orthogonal decomposition images do not necessarily indicate that there are such structures in the flow in steady fashion. This suggests that the spatially periodic structures are generated by a feedback loop in the baseline, but that they are not steady in time.

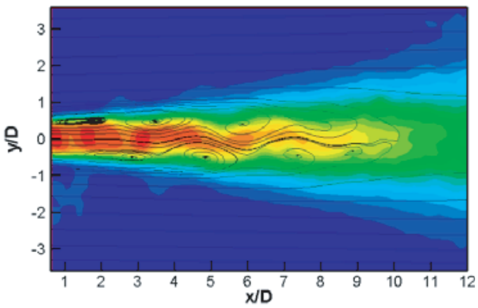

(a) $St_{DF} = 0.26$

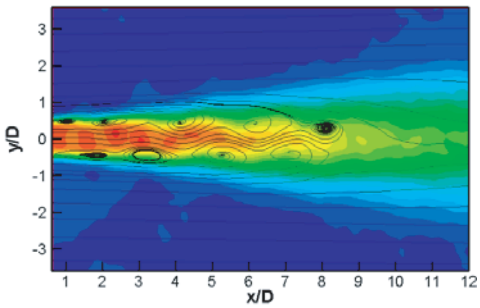

(b) $St_{DF} = 0.33$

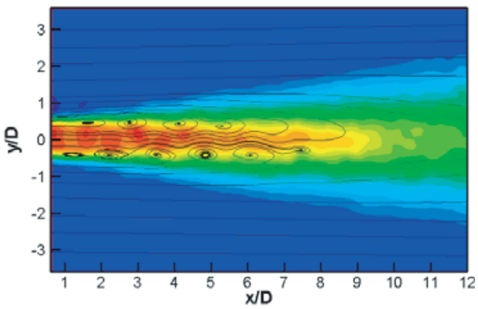

(c) $St_{DF} = 0.52$

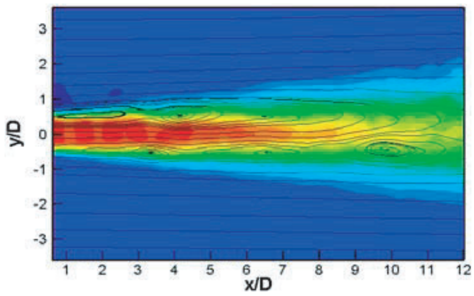

(d) Baseline

Figure 20. Galilean streamlines superimposed on the conditionally-averaged streamwise velocity fields at m = ±1 in the over-expanded $M_J = 1.2$ jet.

There was a sign of competition for energy between generated structures due to forcing and naturally amplified structures at a St_{DF} about 0.3. The indicator of this competition is the behavior of structure spacing especially for m = 0. There is dual spacing of structures around a St_{DF} of 0.3 which suggests competition. The presence of dual spacing at a St_{DF} about 0.3 is observed in Figure 20b. In the upstream region, the spacing is very close to that for the baseline. However, the spacing in the downstream region collapses on the relation in Eq. 1, implying that the structures are generated by forcing. At high St_{DF}'s near 0.8-1.0, the forced structures are small and less energetic so that the naturally amplified structures seem to survive – inferred from the structure spacing. Unlike in the perfectly-expanded jet, the forced structures need to compete with the naturally amplified structures to survive. As a result of this competition or interaction, it is thought that the vortices are weaker than in the perfectly-expanded jet although it is not readily seen in the visualized structures in Figure 20. A careful comparison of Figures 17 and 20 suggests that the generated structures at this St_{DF} are perhaps well organized, but the spanwise dimension is smaller than that observed in the perfectly-expanded M_J = 1.3 jet. These findings suggest that the generated structure in the over-expanded jet is less energetic than those in the perfectly-expanded jet. This reduced strength and growth of the structures may be responsible for the decreased effectiveness in mixing enhancement in the over-expanded jet (Figure 12).

For the under-expanded M_J =1.4 jet, visualized structures at m = ±1 are shown in Figure 22. As was observed in other flow regimes, the spacing and dimension of structures decreased with increasing St_{DF} number. In the baseline jet, there are periodic structures generated by a feedback loop as in the over-expanded jet. The pattern of vortical structures in forced cases is very similar to what was seen in the other two flow regimes of M_J = 1.2 and 1.3 (Figures 17 & 20). At low St_{DF}'s of 0.13 and 0.26, the spacing in the vicinity of the nozzle exit is smaller than that at fardownstream locations. The spacing in the upstream region is actually very close to that for the baseline. As in the over-expanded jet, this dual spacing in the shear layer suggests that the forced structures need to compete with the naturally amplified structures which can be observed in Figure 22f. At moderate St_{DF} numbers of 0.39 and 0.52, only single spacing is seen over the entire streamwise span. A dual spacing is also observed at high St_{DF} numbers about 1.0, but it is not readily observed in Figure 22e.

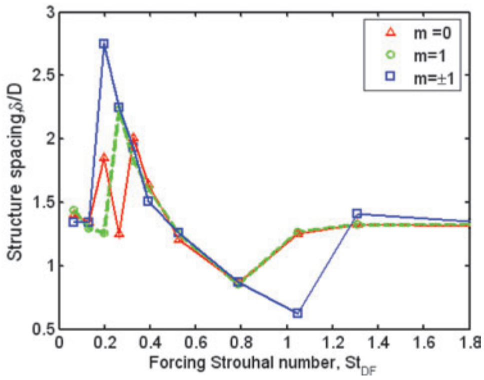

Figure 21. Spacing of the structures in M_J = 1.2 jets.

Although the generated structures appear to be as energetic as those in the perfectly-expanded case, it is expected that the strength of the generated structures will be less in the under-expanded jets due to competition. As in the over-expanded case, the reduced strength may be partially responsible for the reduced jet growth as shown in Figure 14b. At St_{DF} = 0.26, the jet responded to the forcing and the generated structures seem to be more energetic compared to other cases shown in the figure. These energetic structures are responsible for better mixing enhancement as shown in Figure 14b. At St_{DF} = 0.39 and 0.52, the spacing of the generated structures is very close to that of the shock cells. The generated structures are well organized, but it seems that they are not sufficiently energetic to be able to undulate the jet column significantly, as inferred from the relatively straight jet plume. When the jet is forced at high St_{DF}'s as in Figure 22e, the structure spacing is the same as the baseline, but the formation of structures is suppressed by forcing as inferred from the dimension and irregular spacing of the structures. The suppression of naturally amplified structures is most likely responsible for the reduced jet growth and the increased potential core length at high St_{DF}'s (Figure 14b).

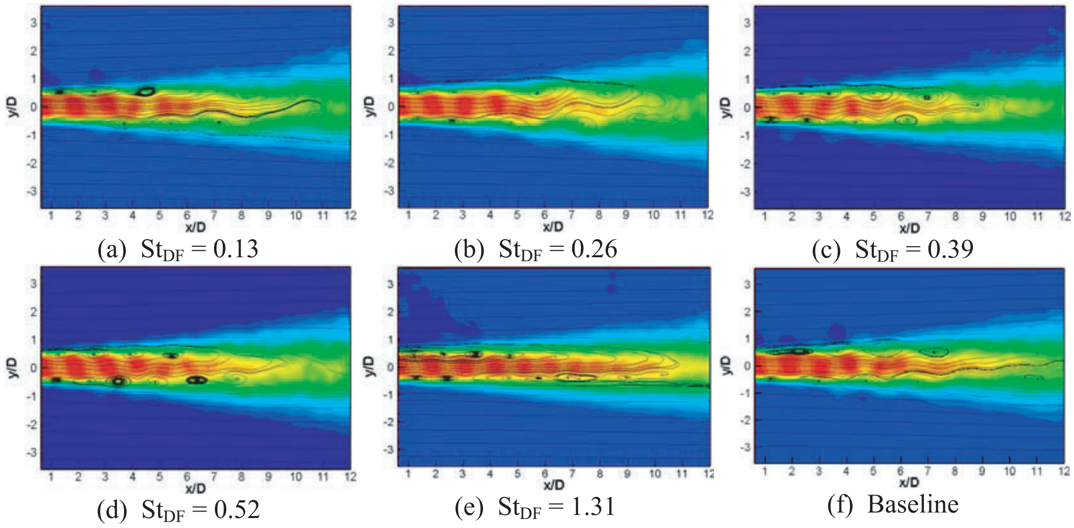

Figure 22. Galilean streamlines superimposed on the conditionally-averaged streamwise velocity fields at $m = \pm 1$ in the under-expanded $M_J = 1.4$ jet.

Figure 23 shows the spacing of periodic structures either forced or naturally amplified. The spacing of generated structures is inversely proportional to St_{DF} numbers ranging roughly from 0.3 to 1.3. For low and high St_{DF} numbers, the structure spacing is the same as that in the baseline jet as was observed in Figure 22. In the M_J =1.4 baseline jet, the Strouhal number at the measured fundamental screech frequency (f_s) is about 0.37 (= $f_s D/U_J$) as shown in Figure 4. This screech and the periodic structures seen in Figure 22f were generated by the feedback loop. As in the over-expanded jet, the initial shear layer at $M_J = 1.4$ is exposed to two sources of perturbation: one is seeded by the plasma actuators and the other is amplified by the flow-acoustic feedback loop. Thus, Figures 22b and 23 suggests that there is a strong competition for energy between these two sets of structures, especially at St_{DF} numbers near 0.3 and 1.0. When the forced structures are not energetic either due to lack of organization (at low St_{DF} numbers) or small in dimension (at high St_{DF} numbers), the naturally amplified structures survive the competition. It seems that the jet responds either to the forcing by the actuators or to the natural perturbation by the flow-acoustic feedback loop. The structure spacing is different from that of the baseline if the jet responds to the perturbation seeded by the actuators.

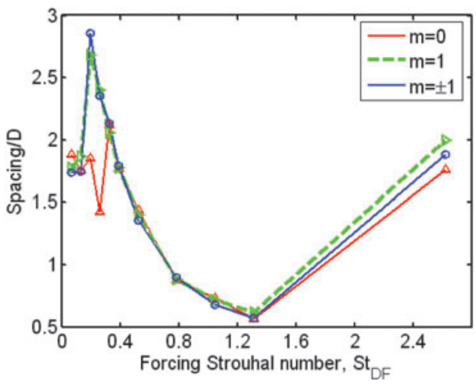

Figure 23. Spacing of structures in $M_J = 1.4$ under-expanded jets.

The jet width for the three baseline/unforced jets is compared as shown in Figure 24. The jet width is increased by the naturally amplified structures in the over- or under-expanded baseline jets. Thus, for imperfectly expanded jets, the reduced mixing enhancement over each baseline jet is partially related to the already enhanced mixing caused by the feedback loop (shown in Figures 10, 12, and 14). At high St_{DF}'s, the jet growth is reduced by forcing at some azimuthal modes (not shown). As discussed earlier, the reduction in jet growth is due to suppression of naturally amplified structures for the imperfectly-expanded jets.

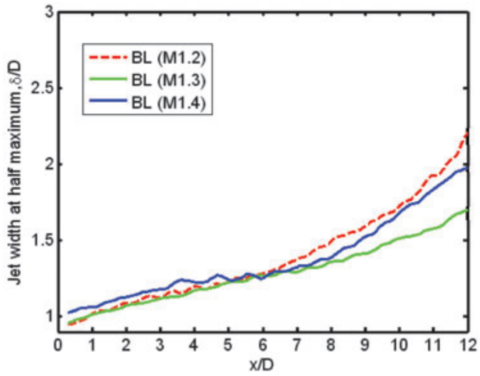

Figure 24. Jet width for the three baseline jets.

4. CONCLUSIONS

Active flow control was used in M_J = 1.2 (over-expanded), 1.3 (perfectly-expanded), and 1.4 (under-expanded) supersonic jets. The Reynolds number based on the jet diameter and jet exit velocity ranged from 1.1×10^6 to 1.4×10^6. The forcing was applied using eight localized arc filament plasma actuators with a forcing Strouhal number ranging from 0.07 to 2.62 for azimuthal modes m = 0-3, ±1, ±2 and ±4. The flow field was measured by a two-component PIV system. The centerline Mach number and jet spreading (using width at half centerline velocity) were used for the evaluation of the overall spreading of the jet. Large-scale structures were visualized to determine their role in jet development.

In the perfectly-expanded M_J = 1.3 jet, the effects of forcing on the structure generation and mixing enhancement were very similar to what had been observed earlier in a M_J = 0.9 subsonic jet. The perfectly-expanded jet responded to the forcing over a wide range of forcing frequencies. The maximum jet spreading occurred when the jet was forced at m = ±1 and $St_{DF} \approx 0.3$. A comparable jet mixing was observed when the jet was forced at m = 1. For the forcing at m = 0, the increase in jet spreading was minimal and the centerline Mach number decayed slower than that of the other two modes.

In the over-expanded (M_J = 1.2) and under-expanded (M_J = 1.4) jets, there were generated structures with a reduced strength compared to those in the perfectly-expanded jet. The reduced strength of the vortical structures is believed to be due to the competition for energy and growth between naturally amplified, due to the flow-acoustic feedback loop, and forced structures. The reduced strength of the generated structures, in turn, is responsible for the relatively reduced jet spreading. For the baseline imperfectly-expanded jets, the jet spreading was increased by the feedback when compared to the perfectly-expanded jet. This is another cause for reduced jet growth in imperfectly-expanded jets since the baseline jet already had increased mixing/spreading due to the feedback. The findings in the present research would be helpful in selecting control strategies in both perfectly- and imperfectly-expanded supersonic jets.

ACKNOWLEDGEMENTS

The support of this research by the Air Force Office of Scientific Research (FA9550-07- 1-0173) with Dr. John Schmisseur is greatly appreciated. The authors would like to thank Igor Adamovich, Munetake Nishihara, and Martin Kearney-Fischer for their help on this work.

REFERENCES

Cho, S.K., Yoo, J.Y., and Choi, H., 1998, "Vortex pairing in an axisymmetric jet using two-frequency acoustic forcing at low to moderate Strouhal numbers," *Experiments in Fluids*, Vol. 25, 305-315.

Cohen, J., & Wygnanski, I. (1987) "The evolution of instabilities in the axisymmetric jet. Part 1. The linear growth of disturbances near the nozzle," *Journal of Fluid Mechanics*, Vol. 176, pp.191-219.

Crow, S.C. and Champagne, F.H., 1971, "Orderly Structure in Jet Turbulences," *Journal of Fluid Mechanics*, Vol. 48, 547-591.

Freymuth, P., 1966, "On On Transition in a Separated Laminar Boundary Layer," *J. of Fluid Mech.*, V. 25, 683-704.

Ginevsky, A.S., Vlasov, Y.V., and Karavosov, R.K., 2004, *Acoustic Control of Turbulent Jets*, Springer-Verlag, Germany, 4-5.

Gutmark, E. and Ho, C.M., 1983, "Preferred Modes and the Spreading Rated of Jets," *Phys. Fluids*, Vol. 26, No. 10, 2932-2938.

Ho, C-M, and Huerre, P., "Perturbed Free Shear Layers," *Ann. Rev. Fluid Mech.*, Vol. 16, pp. 365-424, 1984.

Kastner, J., Kim, J.-H., and Samimy, M., "A Study of the Correlation of Large-scale Structure Dynamics and Far-field Radiated Noise in an Excited Mach 0.9 Jet," *International Journal of Aeroacoustics*, Vol. 8, No. 3, pp. 231-159, 2009.

Kibens, V., 1980, "Discrete Noise Spectrum Generated by Acoustically Excited Jet," *AIAA Journal*, Vol. 18, No. , 434-441.

Kim, J.-H., Kastner, J., Adamovich, I. and Samimy, M., 2007, "Active Control of High Subsonic Jets," *AIAA Paper No. AIAA-2007-0320*.

Kim, J.-H., Kastner, and Samimy, M., 2009, "Active Control of High Subsonic Jets," *AIAA Journal*, Vol. 47, No. 1, 116-128.

Kline, S. J.; Robinson, S. K., "Quasi-coherent structures in the turbulent boundary layer. I – Status report on a community-wide summary of the data," *Near-wall turbulence : 1988 Zoran Zaric Memorial Conference*, Edited by S.J. Kline, N.H. Afgan, 1990.

Melling, A., "Tracer particles and seeding or particle image velocimetry," *Measurement Science and Technology*, Vol. 8, pp. 1406–1416, 1997.

Michalke, A., 1965, "On Spatially Growing Disturbances in an Inviscid Shear Layer," *Journal of Fluid Mechanics*, Vol. 23, 521-544.

Robinson, S. K., Kline, S. J., and Spalart, P. R., A review of quasi-coherent structures in a numerically simulated turbulent boundary layer, NASA technical memorandum, 102191, 1989.

Samimy, M., J., Kim, Kastner, J.-H., Adamovich, I., and Utkin, Y., "Active Control of a Mach 0.9 Jet for Noise Mitigation Using Plasma Actuators," *AIAA Journal*, Vol. 45, No. 4, pp. 890-901, 2007a

Samimy, M., Kim, J.-H., Kastner, J., Adamovich, I., and Utkin, Y., "Active Control of High Speed and High Reynolds Number Jets Using Plasma Actuators," *Journal of Fluid Mechanics*, Vol. 578, pp. 305-330, May 2007b.

Samimy, M. Kastner, J.,, Kim, J.-H., Utkin, Y., Adamovich, I., Bridges, J., and Brown, C., 2006b, "Flow and Noise Control in High Speed and high Reynolds Number Jets Using Plasma Actuators," *AIAA Paper No. 2006-2846*.

Samimy, M., Snyder, R.M., and Kim, J.-H., 2008, "Active Control of Supersonic Jets Operating in Various Flow Regimes," *AIAA Paper No. 2008-0631*.

Utkin, Y., Keshav, S., Kim, J.-H., Kastner, J., Adamovich, I., and Samimy, M., 2007, "Use of Localized Arc Filament Plasma Actuators for High Speed Jet Control," *Journal of Physics D: Appl. Phys.* Vol. 40 No 3, 685-694.

Zaman, K.B.M.Q. and Hussain, A.K.M.F., 1981, "Turbulence Suppression in Free Shear Flows by Controlled Excitation," *J. Fluid Mechanics*, Vol. 103, 133-159.